NHXM active shielding trade-off study: Box model

V. Fioretti[1,2], A. Bulgarelli[1], V. Bianchin[1], M. Trifoglio[1], F. Gianotti[1] and G. Malaguti[1]
[1)]INAF/IASF Bologna, [2)]University of Bologna, Astronomy Department

INAF/ IASF – Bologna Technical Report n. 593/2011

Change history

Version	Date	Notes
1.0	Sept. 9th, 2010	1st Issue
1.1	Sept. 13th, 2010	2nd Issue
1.2	Dec. 3rd, 2010	3th Issue
2.0	Jul. 14th, 2011	4th Issue

1. Introduction

The New Hard X-ray Mission (NHXM) is a space mission [1] proposed by a joint European team to the ESA medium mission call in 2010. It will be equipped with four broad band (0.5 – 80 keV) grazing incidence X-ray mirrors [2], with a 10 m focal length, achieved after the launch by means of a deployable structure. Three of the four telescopes will have at their focus identical high angular resolution (<20" HEW) spectral-imaging cameras, achieving a sensitivity < 1 μCrab (3σ, T = 1 Ms) at 10 – 40 keV, as defined by the top scientific requirements. The mission is planned to operate in a low inclination (<5 deg.), circular low Earth orbit (LEO), at an altitude of about 550 km. Since the minimum detectable flux depends on the square root of the total background level, the minimization of the background flux on the NHXM focal plane is a key requirement to achieve the scientific objectives.
The results presented here are part of a comprehensive simulation and trade-off analysis of the NHXM shielding system performed at the INAF/IASF Bologna Institute.

2. Shielding system analysis: the simplest model

In order to fully characterize the LEO radiation effects on the shielding and detector response, we developed an extremely simplified, box shaped shielding system surrounding a monolithic LED and HED assembly based on the NHXM focal plane design. Given the simplified geometry, the results presented here are not the expected NHXM background count rate but they represent a first, fundamental step to select the major sources of background and, consequently, to optimize the shielding system. In particular, the anticoincidence (AC) count rate strongly affects the observation dead time for a frame-by-frame detection read out. The baseline shielding concept, already employed in the NHXM001 Geant4 geometry release, is composed by a plastic scintillator (active shield) surrounding a graded passive shielding. In the present work, the background simulation is performed for three shielding configurations:

- Active shielding (plastic scintillator) surrounding the passive shielding (baseline design, defined as Case A);
- Active shielding (plastic scintillator) enclosed by the passive shielding (defined as Case B);
- Active shielding (inorganic scintillator) enclosed by the passive shielding (defined as Case C).

The use of organic scintillators as active shield allows to reduce the mass budget, thanks to the lighter components, with no secondary activation lines and an higher feasibility respect to inorganic (BGO, NaI) anticoincidence systems, which in turn ensure an higher absorption efficiency.
The choice between an organic and inorganic active shield should follow a detailed analysis of the background and AC count rate as a function of the AC threshold, with a parallel comparison of the background spectra. For this reason, the third configuration (Case C) uses an inorganic scintillator as active shield, to be compared to the Case B configuration..
The simulation results are compared with the aim of selecting the active shield design that ensures the best response in terms of background and active shield count rate, given the space radiation environment of the NHXM mission.

3. Sources of background

The sources of "prompt" (not due to delayed events) background expected in a LEO, low inclination orbit, and used as input in the Geant4 simulation, are:

- Cosmic X-ray Background (CXB);
- Earth X-ray Albedo;
- primary (Cosmic Rays) and albedo protons;
- albedo electrons;
- albedo positrons.

The spectral distribution of the particles used as input in the present background evaluation is plotted in Fig. 2.

3.1 Photonic component

The CXB flux, with an energy density peaking in the 20 - 40 keV energy band, is simulated from 1 keV to 100 MeV, using the spectral shape of [3]. The CXB and Cosmic Rays (CR) flux is significantly shielded by the Earth, which, for a 550 km altitude spacecraft, covers about the 30% of the sky. The Earth atmosphere, on the other hand, emits in the X-ray band because of the CXB reflection by the atmospheric upper layers and as induced by CR interactions [4].
Figure 1 (left panel) shows a collection of the Earth X-ray albedo observations from literature (extended up to 1 MeV), expressed in terms of surface brightness: the continuous red and green lines model the INTEGRAL observation as published by respectively [4] and [5], the blue line refers to the Swift/BAT observation [6] while the black line shows the CXB flux for comparison.
Since the CXB flux is isotropic, the intensity of its reflection does not depend on the telescope point of view. The CR flux, instead, is energetically cut off by the Earth magnetic field, with a lower energy (geomagnetic rigidity) that depends on the field intensity. From high (~60 deg.) to low (~20 deg.) latitudes in the near-Earth region, the energy cut off ranges from ~100 MeV to ~10 GeV. As a result, the Earth X-ray albedo intensity decreases from polar to equatorial observations, as shown by the gap between the INTEGRAL (~50 deg. Inclination orbit) and the BAT (~20 deg. inclination orbit) albedo intensity in Fig. 1 (left panel). The CR induced albedo equation developed by [8] can be used to model the Earth X-ray albedo as seen by NHXM, i.e. for an equatorial, 550 km high orbit. Figure 1 (right panel) shows the computed total X-ray albedo, for a minimum solar activity, as seen from a 0 deg. (NHXM, red line) and 20.6 deg. (Swift, blue line) inclination orbit, while the dotted black line refers to the modelled CXB reflection and the continuous black line to the Swift/BAT observation. Since the BAT model (blue line) reproduces with good accuracy the real spectrum (black line), the NHXM X-ray albedo (red line) can be assumed as model in the background simulation.

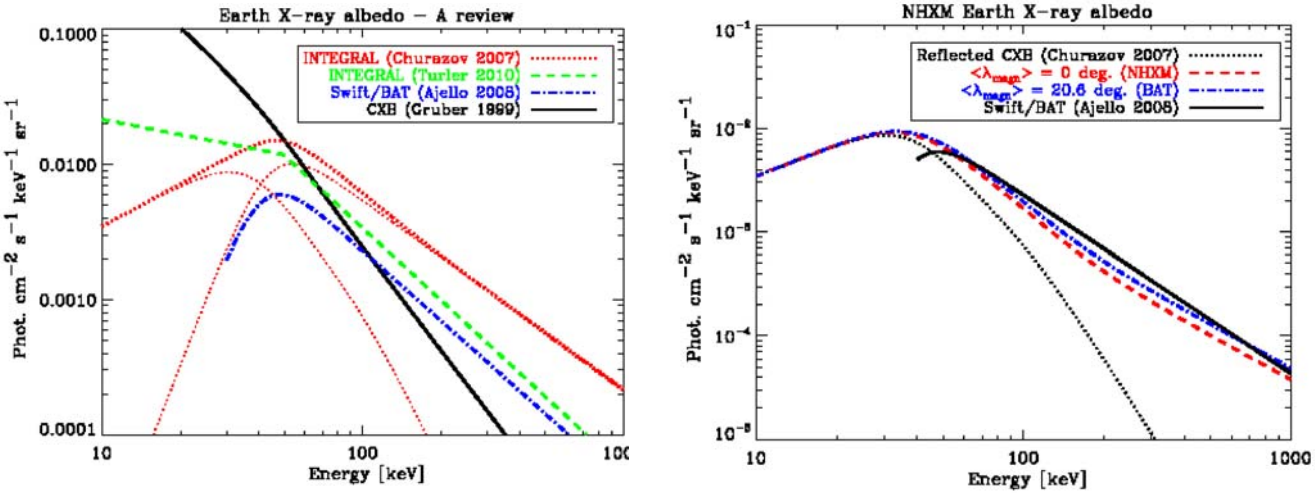

Figure 1: *Left*: Earth X-ray albedo as observed by INTEGRAL (red [4] and green [5] line) and Swift/BAT [6], while the dotted red lines show the decomposition in CXB reflection and CR interactions for the [4] observation and the black line is the CXB flux for comparison. *Right*: total X-ray albedo computation for NHXM (red line) and Swift (blue line) orbit; the latter is shown in comparison with the real Swift/BAT observation (red line), while the dotted black line refers to the CXB reflection, which contributes to the total computed albedo.

3.2 Charged particles component

Since the galactic CR flux is composed of about 98% nuclei (87% Hydrogen, 12% Helium and 1% heavier nuclei) and 2% leptons (>90% electrons) [10, 11], the contribution of primary electrons and positrons to the background is neglected.

The simulated proton flux is the sum of the primary CR and the secondary albedo protons induced by CR interactions with the atmosphere, as observed by the AMS [12] in June 1998 during solar minimum (modulation parameter Φ = 400 MV according to [13]). The geomagnetic rigidity for a magnetic latitude of 5 deg. (the Earth equator) and an altitude of 550 km is about 15 GV (at solar minimum), resulting, following the computation of [9], in a lower energy cut off of 14 GeV for protons. Below this energy, the albedo charged particles flux arises, as a consequence of CR interaction with air nuclei initiating nuclear interactions cascades with the final result of producing secondaries protons, electrons and positrons at relatively low energies.
These secondary charged particles are usually classified in splash, or leaking, albedo if emerging from the atmosphere, while the term reentrant albedo denotes downward moving particles below the geomagnetic cut off, travelling backward along the magnetic field line connected to the point of observation. There is also a fraction of secondary particles that can remain trapped for several years, bouncing several times in the magnetic field. The intensity of splash and reentrant albedo is expected to be of the same order [12], especially at low latitudes. For this reason, albedo protons, electrons and positrons are simulated isotropically from 4π sr. Since primary and secondary protons are simulated as an unified flux, the CR flux is also simulated without taking into account the Earth shielding.

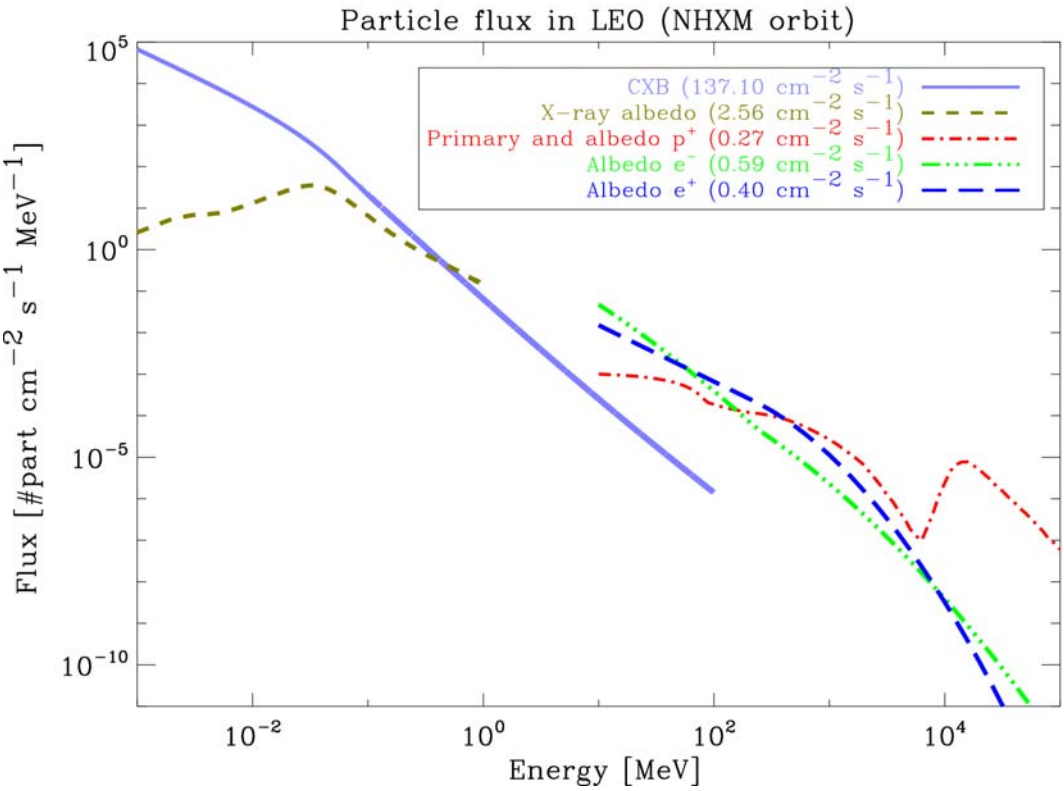

Figure 2: Overview of the simulated space radiation environment, normalized for the subtended solid angle. *Light blue*: CXB (1 keV – 100 MeV); *Olive green*: Earth X-ray albedo (1 keV – 1 MeV); *red*: primary and secondary protons (10 MeV – 100 GeV); *light green*: albedo electrons (10 MeV – 80 GeV); *dark blue*: albedo positrons (10 MeV – 80 GeV).

4. Geant4 mass model

The Geant4 camera geometry model is composed by:

- NXHM focal plane:
  A Silicon Low Energy Detector (LED), 0.45 mm thick, over a CdTe High Energy Detector (HED), 1.5 mm thick.
- Box-shaped active and passive shielding system totally surrounding the focal plane.

The LED and HED are simulated by single, not-pixellated volumes: a 57×57×0.45 mm thick Silicon

(Si) layer, the LED, and a 50×50×1.5 mm thick Cadmium Telluride (CdTe) layer, the HED, separated by a 1.2 cm distance. The distance between the detectors and the shielding walls on top and bottom sides is 10 cm, so that the surrounding box height is 21.2 cm, with a side of 25 cm (see Fig. 3).

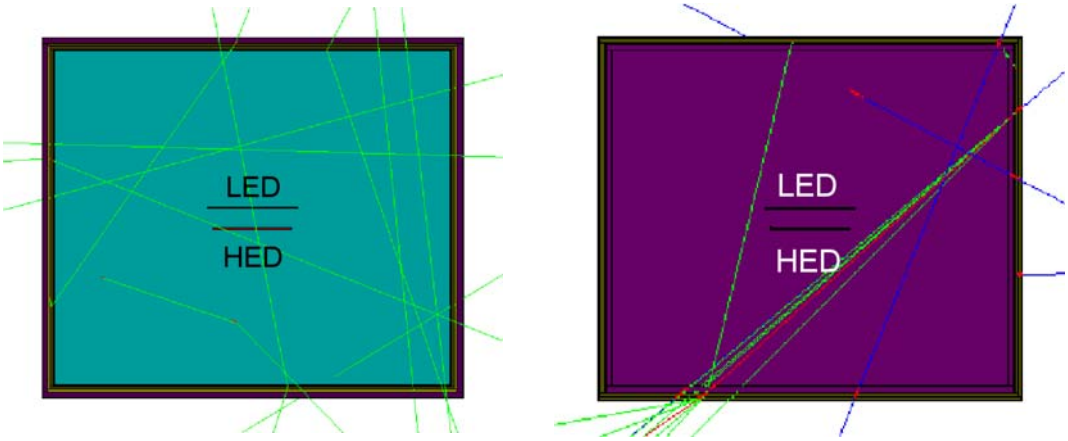

Figure 3: Cut view of the Geant4 mass model with the AC surrounding the passive shielding (left panel) and enclosed by the passive layers (right panel). The green, blue and red lines being the trajectories of the interacting photons, protons and electrons respectively.

The materials composing the plastic and inorganic active shielding are Polystyrene and NaI respectively, with a thickness of 3.8 mm for all the studied configurations.
The passive shielding is graded with a main absorber made of Tantalum. For a detailed trade-off analysis of the passive shielding efficiency on the background rejection see Bianchin et al. (in prep.).
The thickness and composition of each layer is listed in the following table:

Material	Z	Kα, Kβ [keV]	t [mm]
Tantalum (Ta)	73	57.5, 65.2	1.5
Tin (Sn)	50	23.5, 28.5	2.2
Copper (Cu)	29	8.1, 8.9	0.48
Aluminum (Al)	13	1.5, 1.6	0.27
Carbon (C)	6	0.28, /	0.1

Table 1: Materials and thicknesses of the graded passive shield.

An event is removed if the same primary particles generates an event in the active shield (an energy deposit above the lower energy threshold) and a LED (or HED) count within the detection energy range. All the results presented here refer to an AC threshold of 200 keV.

5. The background in a Box

The development of the Geant4 mass model, the Monte Carlo simulation and the background analysis are performed by means of the BoGEMMS tool [Bulgarelli et al. in prep.].
The simulation output is normalized according to [14]. Background spectra are produced in the 0.5 – 20 keV energy range for the LED and in the 5 – 100 keV energy range for the HED, while the background level is evaluated as the average level of counts per unit of detector area and time along the reported operative energy ranges.
The events that produce an energy deposit, within the selected energy range, on both LED and HED are removed, since they are classified as a separate group of events in the standard data analysis. The reported errors refer to the Monte Carlo simulation, without taking into account the detector electronic fluctuations, and are computed following the Poisson statistics.

5.1 Energy averaged background levels

AC (plastic) surrounding the passive shield (baseline design):

Case A		Background count rate [cts cm^{-2} s^{-1} keV^{-1}]			
Input	Det.	AC + Passive shield		Triggered counts	AC rate [cts s^{-1}]
		AC off	AC on		
CXB	LED	$(1.48\pm0.11)\times10^{-5}$	$(1.43\pm0.11)\times10^{-5}$	3.1%	6.4
	HED	$(5.09\pm0.10)\times10^{-5}$	$(5.00\pm0.10)\times10^{-5}$	1.8%	
Protons	LED	$(1.53\pm0.02)\times10^{-4}$	$(0.30\pm0.10)\times10^{-6}$	99.8%	185.4
	HED	$(2.36\pm0.01)\times10^{-4}$	$(0.33\pm0.05)\times10^{-6}$	99.9%	
Electrons	LED	$(1.81\pm0.04)\times10^{-4}$	0	100%	411.1
	HED	$(4.21\pm0.03)\times10^{-4}$	0	100%	
Positrons	LED	$(2.10\pm0.03)\times10^{-4}$	$(0.18\pm0.09)\times10^{-6}$	99.9%	273.2
	HED	$(4.70\pm0.02)\times10^{-4}$	$(0.45\pm0.07)\times10^{-6}$	99.9%	
X-ray Albedo	LED	$(1.14\pm0.03)\times10^{-5}$	$(1.06\pm0.02)\times10^{-5}$	6.9%	5.4
	HED	$(3.78\pm0.02)\times10^{-5}$	$(3.53\pm0.02)\times10^{-5}$	6.6%	
Total	LED	$(5.68\pm0.10)\times10^{-4}$	$(0.25\pm0.09)\times10^{-4}$	/	881.5
	HED	$(1.22\pm0.01)\times10^{-3}$	$(0.86\pm0.01)\times10^{-4}$		

Table 2: Background level, in counts cm^{-2} s^{-1} keV^{-1}, the fraction of the triggered events, and the AC count rate, in counts s^{-1}, for the Case A geometry configuration.

Passive shield enclosing the AC (plastic):

Case B		Background count rate [cts cm^{-2} s^{-1} keV^{-1}]			
Input	Det.	AC + Passive shield		Triggered counts	AC rate [cts s^{-1}]
		AC off	AC on		
CXB	LED	$(1.58\pm0.11)\times10^{-5}$	$(1.30\pm0.10)\times10^{-5}$	17.9%	5.5
	HED	$(4.94\pm0.10)\times10^{-5}$	$(4.52\pm0.10)\times10^{-5}$	8.6%	
Protons	LED	$(2.14\pm0.03)\times10^{-4}$	$(0.36\pm0.10)\times10^{-6}$	99.8%	148.0
	HED	$(2.53\pm0.01)\times10^{-4}$	$(0.76\pm0.08)\times10^{-6}$	99.7%	
Electrons	LED	$(2.35\pm0.04)\times10^{-4}$	$(2.69\pm0.13)\times10^{-5}$	88.6%	177.1
	HED	$(4.88\pm0.03)\times10^{-4}$	$(8.77\pm0.12)\times10^{-5}$	82.0%	
Positrons	LED	$(2.69\pm0.03)\times10^{-4}$	$(1.50\pm0.08)\times10^{-5}$	94.5%	178.8
	HED	$(5.33\pm0.03)\times10^{-4}$	$(4.60\pm0.07)\times10^{-5}$	91.4%	
X-ray albedo	LED	$(1.29\pm0.03)\times10^{-5}$	$(1.04\pm0.02)\times10^{-5}$	19.4%	4.4
	HED	$(3.95\pm0.03)\times10^{-5}$	$(3.50\pm0.02)\times10^{-5}$	11.4%	
Total	LED	$(7.47\pm0.11)\times10^{-4}$	$(0.66\pm0.04)\times10^{-4}$	/	513.8
	HED	$(1.36\pm0.01)\times10^{-3}$	$(2.15\pm0.03)\times10^{-4}$		

Table 3: Background level, in counts cm^{-2} s^{-1} keV^{-1}, the fraction of the triggered events, and the AC count rate, in counts s^{-1}, for the Case B geometry configuration.

Passive shield enclosing the AC (NaI):

Case C		Background count rate [cts cm^{-2} s^{-1} keV^{-1}]			
Input	Det.	Passive shield + AC		Triggered counts [%]	AC rate [cts s^{-1}]
		AC off	AC on		
CXB	LED	(1.71±0.16)×10^{-5}	(1.06±0.13)×10^{-5}	38.4%	35.0
	HED	(4.75±0.14)×10^{-5}	(3.38±0.12)×10^{-5}	28.8%	
Protons	LED	(1.80±0.04)×10^{-4}	(0.20±0.14)×10^{-6}	99.9%	148.1
	HED	(2.69±0.03)×10^{-4}	(0.64±0.13)×10^{-6}	99.8%	
Electrons	LED	(1.88±0.11)×10^{-4}	(0.66±0.21)×10^{-5}	96.5%	247.4
	HED	(4.41±0.09)×10^{-4}	(2.84±0.22)×10^{-5}	93.6%	
Positrons	LED	(2.49±0.10)×10^{-4}	(0.44±0.14)×10^{-5}	98.2%	216.0
	HED	(5.55±0.08)×10^{-4}	(1.71±0.14)×10^{-5}	96.9%	
X-ray albedo	LED	(1.19±0.04)×10^{-5}	(0.70±0.03)×10^{-5}	40.8%	25.6
	HED	(3.65±0.03)×10^{-5}	(2.35±0.03)×10^{-5}	35.7%	
Total	LED	(6.46±0.28)×10^{-4}	(0.29±0.05)×10^{-4}	/	672.1
	HED	(1.35±0.02)×10^{-3}	(1.03±0.05)×10^{-4}		

Table 4: Background level, in counts cm^{-2} s^{-1} keV^{-1}, the fraction of the triggered events, and the AC count rate, in counts s^{-1}, for the Case C geometry configuration.

5.2 Background spectra

The background spectra as obtained with a plastic AC placed inside the passive shielding (Case B) are presented in Fig. 4 (LED) and 5 (HED). The total level, given by the sum of all the simulated sources, is shown in black. For a comparison of the three tested configuration, see Sec. 5.3.
The background spectral distribution is dominated by the continuum, with no evidence for fluorescence lines, and the overall shape is constant. As expected, the photonic component is only slightly affected by the AC triggering, while the protons are efficiently removed. However, the charged particles induced background also dominates after the removal of the AC events because of the counts generated by the electrons and positrons, reaching a level close the requirement in the HED.

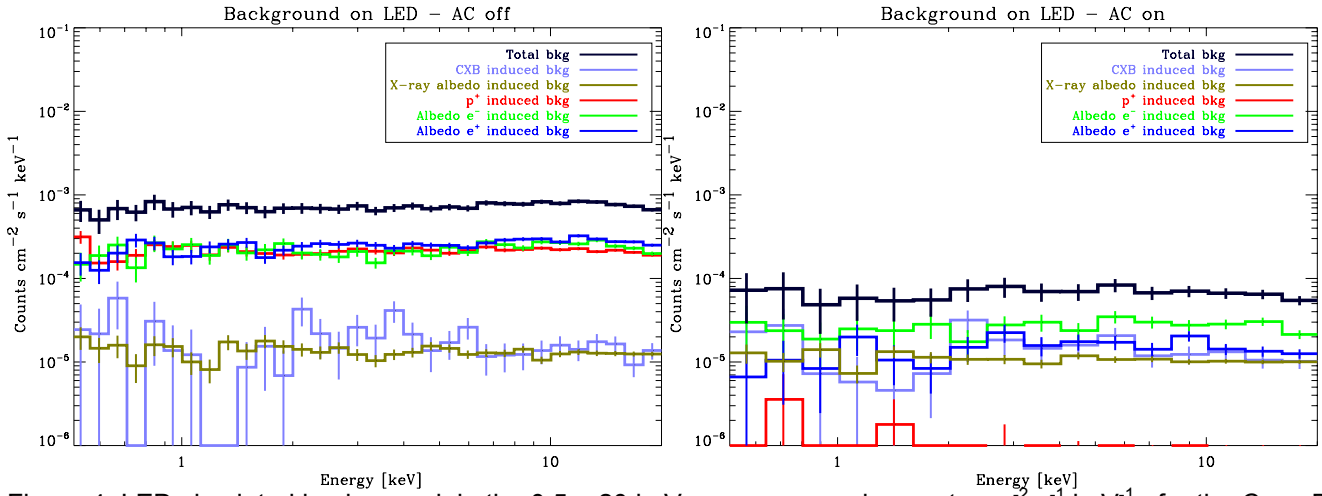

Figure 4: LED simulated background, in the 0.5 – 20 keV energy range, in counts cm^{-2} s^{-1} keV^{-1}, for the Case B configuration in “AC off” (left) and “AC on” (right) mode.

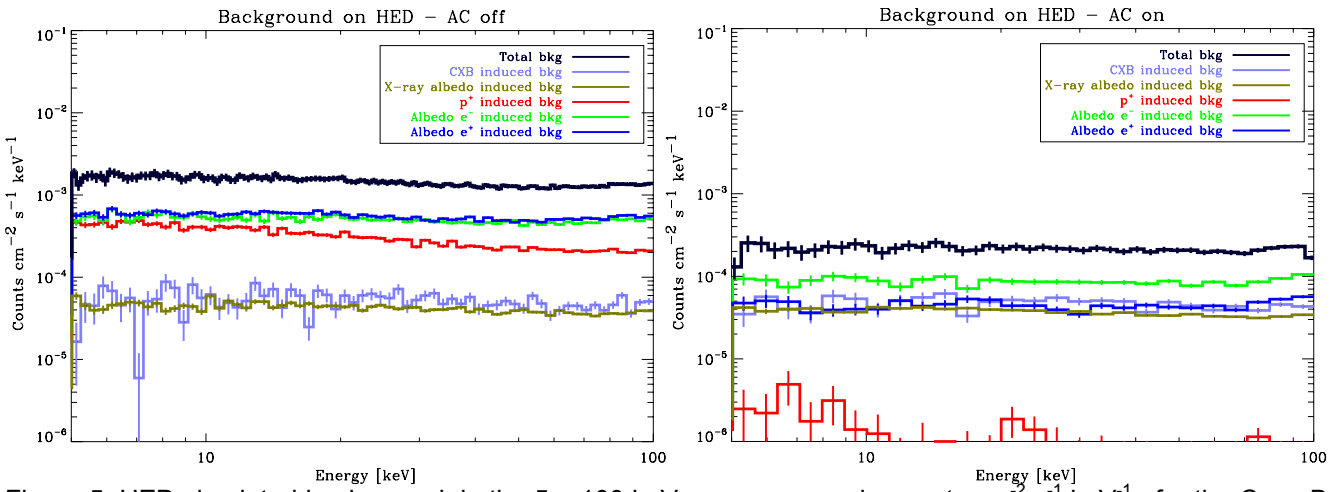

Figure 5: HED simulated background, in the 5 – 100 keV energy range, in counts cm^{-2} s^{-1} keV^{-1}, for the Case B configuration in "AC off" (left) and "AC on" (right) mode.

This is not the case if the plastic AC is placed externally to the passive shielding: the background level induced by the charged particles, including electrons and positrons, is well below the requirement (see Fig. 7, right panel). This results implies that the presence of passive, highly absorbing material outside the AC generates a cascade of secondaries that can not be efficiently removed by the internal AC.
If an inorganic, in this case NaI, active shield is placed within the passive shield, the efficiency on removing electrons and positrons induced events increases, with a related background level about half the Case B configuration (see, again, Fig. 7, right panel).
The problem with the use of an NaI scintillator is that intense Iodium fluorescence lines arise, as shown in Fig. 6 (the HED background spectra for the Case C). The bump below 6 keV visible in the "AC off" mode is the sum of escape peaks emission lines, also arising at 9 keV. It must be pointed out that in the Case C configuration the NaI is placed close to the detectors without any passive shielding to absorb its fluorescence emission.

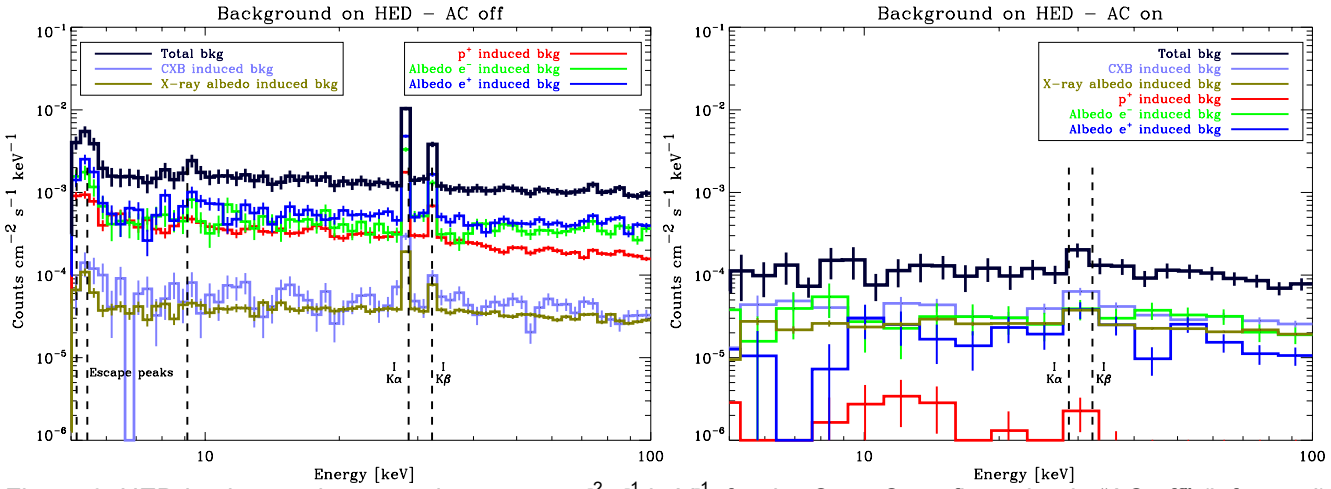

Figure 6: HED background spectra, in counts cm^{-2} s^{-1} keV^{-1}, for the Case C configuration in "AC off" (left panel) and "AC on" (right panel) mode.

5.3 Comparison of the tested configurations

The energy averaged background levels in the 0.5 -20 keV (LED) and 5 – 100 keV (HED) energy ranges are compared in Fig. 7 for the three tested configurations. According to the present mission design, the LED count rate is not filtered by the AC triggering, so that the maximum background level, defined by the top scientific requirements, is 1×10^{-3} counts cm^{-2} s^{-1} keV^{-1} in "AC off" mode. The AC counts are instead removed from the HED detection, so that its maximum background level, 2×10^{-4}

counts cm^{-2} s^{-1} keV^{-1}, must be intended in “AC on” mode. Both requirements are labelled by horizontal dashed lines.

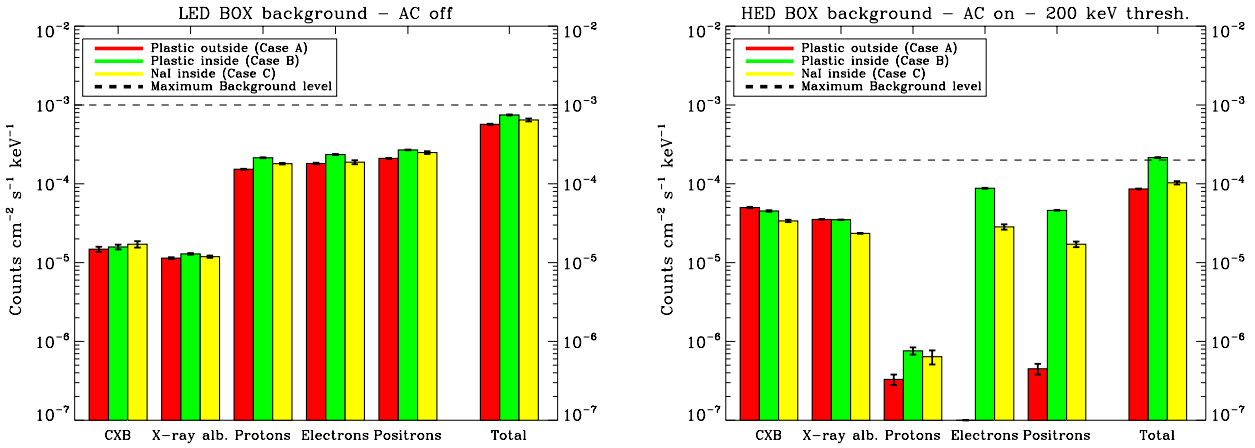

Figure 7: LED (left panel) and HED (right panel) background count rate in “AC off” and “AC on” mode respectively for a plastic active shield outside (red columns, Case A) and inside (green columns, Case B) the passive system. The yellow columns instead refer to the background level obtained by using an NaI scintillator as internal active shield (Case C). The horizontal line shows the NHXM accepted background level.

The three configurations do not extremely differ in terms of resulting background level for the LED instrument, since the AC triggering is not applied. The Case B, with the plastic AC inside, results in a background increase of about 50% respect to the Case A. The charged particles induced background is about an order of magnitude higher than the photonic background, as expected.
If we turn on the AC, the scenario changes, as visible in the HED plot of Fig. 7, right panel. The photonic background decreases of about 50% if the NaI is applied, but the CXB and X-ray albedo photons are not strongly affected by the AC. The charged particles are instead affected by the AC design, with a background level that falls off if the plastic AC is placed outside the passive shield (Case A). As previously noted, the external passive material decreases the AC efficiency to remove charged particles, an effect especially visible for the Case B, that results in a total background level about 2 times higher than the Case C, sharing the same geometry but using an inorganic AC.
It must underlined that the AC, even if placed outside the passive shielding, would be surrounded by additional passive material due to the external case and the payload itself, so that an increase in the electron and positron induced background should be expected in the Case A configuration.

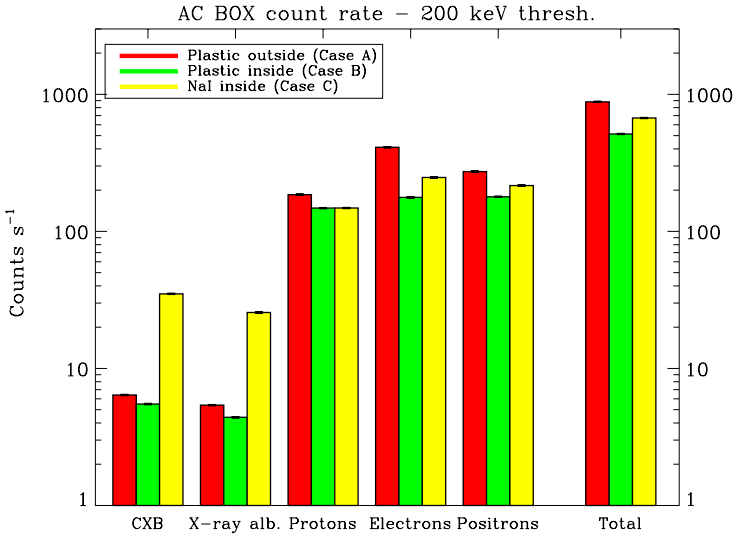

Figure 8: AC count rate induced by each class of input particle and the total value.

The Case B design results in the highest background level, but also in the lowest total AC count rate, as shown in Fig. 8, ranging between 880 (Case A) and 510 (Case B) counts s^{-1}. As expected, the NaI presents the highest efficiency in removing the photonic background, so that the induced AC count rate is higher.
The Case C design, with the NaI shield placed inside the passive material, results to be the best configuration in terms of background/AC count rate performances, but it also causes intense fluorescence lines in the HED background spectra, so that an additional layer of passive material, with high photoelectric cross section in the energy range of interest, is needed.

6. Conclusions

- Background spectral analysis:
  - The overall shape is constant for both LED and HED;
  - There is no evidence of fluorescence emission from the passive layers.

- Plastic vs inorganic scintillator as active shield:
  - The NaI is more efficient in removing both photons and charged particles, resulting in a total background level 2 times lower while keeping a comparable AC count rate;
  - Intense fluorescence lines and escape peaks are detected by the HED if the NaI is applied.

- Effect of the passive shielding on the anticoincidence count rate:
  - The presence of external passive shielding generates a wealth of secondaries of lower energy to the AC decreasing its efficiency in removing the sources of background, in particular electrons and positrons;
  - As a direct consequence, the AC count rate is lower if the passive shield is placed outside.

7. References

1. Tagliaferri G. et al., “NHXM: a New Hard X-ray imaging and polarimetric Mission”, in Proc. of SPIE, Vol. 7732
2. Pareschi G. et al., “Design and development of the optics system for the NHXM Hard X-ray and Polarimetric Mission”, in Proc. of SPIE, Vol. 7437
3. Gruber D. E. et al., “The Spectrum of Diffuse Cosmic Hard X-Rays Measured with HEAO-1”, 1999, ApJ, 520, 124
4. Churazov E. et al., “INTEGRAL observations of the cosmic X-ray background in the 5–100 keV range via occultation by the Earth”, 2007, A&A, 467, 529
5. Turler M. et al., “INTEGRAL hard X-ray spectra of the cosmic X-ray background and Galactic ridge emission”, 2010, A&A, 512, 49
6. Ajello M. et al., “Cosmic X-ray background and Earth albedo spectra with SWIFT BAT”, 2008, ApJ, 689, 666
7. Churazov E. et al., “Earth X-ray albedo for cosmic X-ray background radiation in the 1–1000 keV band”, 2008, MNRAS, 385, 719
8. Sazonov S. et al., “Hard X-ray emission of the Earth’s atmosphere: Monte Carlo simulations”, 2007, MNRAS, 377, 1726
9. Gehrels N., “Instrumental background in gamma-ray spectrometers flown in low Earth orbit”, 1992, NIM-A, 313, 513
10. Simpson J. A., "Elemental and Isotopic Composition of the Galactic Cosmic Rays”, 1983, Ann. Rev. Nucl. Part. Sci., 33, 323
11. Adriani O. et al., “Positrons and Electrons in Primary Cosmic Rays As Measured in the PAMELA Experiment”, 2009, Bulletin of the Russian Academy of Sciences, 73, 568
12. Alcaraz J. et al. (AMS collaboration), “Protons in near Earth orbit”, 2000, Phys. Lett. B, 472, 215
13. Wiedenbeck M.E. et al., “The Level of Solar Modulation of Galactic Cosmic Rays from 1997 to 2005 as Derived from ACE Measurements of Elemental Energy Spectra”, 2005, International Cosmic

Ray Conference Pune, 00, 101
14. Fioretti V. and Malaguti G., “Simbol-X Geant4 background simulation: on the geometrical model of an isotropic flux in space”, INAF/IASF Bologna Internal Report 2009